

## A low-frequency sound absorbing material with subwavelength thickness

Changru Chen, Zhibo Du, Gengkai Hu, and Jun Yang

Citation: *Appl. Phys. Lett.* **110**, 221903 (2017);

View online: <https://doi.org/10.1063/1.4984095>

View Table of Contents: <http://aip.scitation.org/toc/apl/110/22>

Published by the [American Institute of Physics](#)

---

### Articles you may be interested in

[Sound transmission through an acoustic porous metasurface with periodic structures](#)  
*Applied Physics Letters* **110**, 171904 (2017); 10.1063/1.4982633

[A broadband acoustic metamaterial with impedance matching layer of gradient index](#)  
*Applied Physics Letters* **110**, 241903 (2017); 10.1063/1.4986472

[Acoustic metasurface-based perfect absorber with deep subwavelength thickness](#)  
*Applied Physics Letters* **108**, 063502 (2016); 10.1063/1.4941338

[Acoustic broadband metacouplers](#)  
*Applied Physics Letters* **110**, 203504 (2017); 10.1063/1.4983674

[Perfect absorption of low-frequency sound waves by critically coupled subwavelength resonant system](#)  
*Applied Physics Letters* **110**, 023502 (2017); 10.1063/1.4973925

[Ultra-thin metamaterial for perfect and quasi-omnidirectional sound absorption](#)  
*Applied Physics Letters* **109**, 121902 (2016); 10.1063/1.4962328

---

**Scilight**

Sharp, quick summaries **illuminating**  
the latest physics research

Sign up for **FREE!**



## A low-frequency sound absorbing material with subwavelength thickness

Changru Chen,<sup>1</sup> Zhibo Du,<sup>1</sup> Gengkai Hu,<sup>1,a)</sup> and Jun Yang<sup>2</sup>

<sup>1</sup>School of Aerospace Engineering, Beijing Institute of Technology, Beijing 100081, China

<sup>2</sup>Department of Mechanical and Materials Engineering, The University of Western Ontario, London, Ontario N6A 5B9 Canada

(Received 18 January 2017; accepted 12 May 2017; published online 31 May 2017)

We propose a sound absorbing material efficient for low frequency. This material is mainly composed of two axially coupled tubes in series, which are co-planarly coiled in a plane perpendicular to incident waves. By carefully designing the geometric parameters of the coupled tubes, we can overlap the absorption coefficient curves of each individual tube and are therefore able to broaden the frequency bandwidth within which the absorption coefficient is larger than a designed value. A material with an absorption coefficient greater than 0.8 over a frequency bandwidth of 36 Hz for a low frequency of around 100 Hz can be designed, and the wavelength to thickness ratio reaches as high as 38.5. The experiment measurement with the sample made by the 3D printing technique is also conducted to validate the proposed design method. This work may stimulate the research studies on and applications for low frequency sound absorption. *Published by AIP Publishing.* [<http://dx.doi.org/10.1063/1.4984095>]

Low-frequency sound absorption is a challenging problem in engineering due to weak sound energy dissipation in the case of long wavelength.<sup>1</sup> Traditional sound absorbing materials (SAMs), such as porous materials, micro-perforated plates, or sound absorption wedges, show poor absorption performance for low frequency sound.<sup>2–10</sup> To enhance the coupling between sound and SAMs, different methods have been proposed, such as graded porous material, multilayered structure, or material microstructure optimization.<sup>11,12</sup> Sound absorption performance could be improved to some extent using these methods; however, we still encounter many difficulties in reducing the sample size.

A thin film metamaterial could stop low frequency sound by reflection through negative mass effects,<sup>13,14</sup> and its sound absorption coefficient is however bound by a theoretical limit of 50%.<sup>15</sup> By coupling a thin film with an air cavity at resonant frequency, the thin film metamaterial is able to consume a large amount of sound energy at a designed frequency,<sup>14–20</sup> but the sound absorption bandwidth is narrow and limited only to the designed resonant frequency.

In recent years, the method of coiling up space has been proposed to achieve extreme acoustic properties by increasing the sound path.<sup>21–25</sup> When coiling up a quarter-wave resonator in a plane perpendicular to incident waves, a sub-wavelength sound absorption panel has been designed with a total absorption at the resonant frequency.<sup>26,27</sup> However, this sound absorption material works only in a very narrow frequency range around the designed resonant frequency. More recently, a broadband sound absorbing structure is proposed by varying the length of side resonators in parallel,<sup>28</sup> the operating wavelength to sample thickness ratio may reach.<sup>13–17</sup>

Inspired by these works, we propose a different structure of subwavelength scale, which has a good sound absorption

performance within an extremely low frequency range. The basic idea is coiling up two axially coupled tubes in series into a layer perpendicular to incident waves for reducing the sample thickness. By carefully designing the geometry of the two axially coupled tubes, we can overlap the absorption curves of the individual tubes and broaden the frequency bandwidth for sound absorption.

The proposed sound absorbing material consists of designed unit cells, as illustrated in Fig. 1(a). The unit cell is composed of a front panel, an intermediate layer, and a back wall, as shown in Fig. 1(b). The thin front panel is equipped with a cut-through pore or circular shape to let in acoustic waves. The intermediate layer consists of two axially coupled tubes in series coiled up in a plane perpendicular to incident waves. The back wall is a thin back terminal preventing sound leakage.

The frequency and bandwidth of the sound absorption coefficient for the proposed material are closely related to the geometric parameters of the two axially coupled tubes. In the following, we assume the sound hard boundary

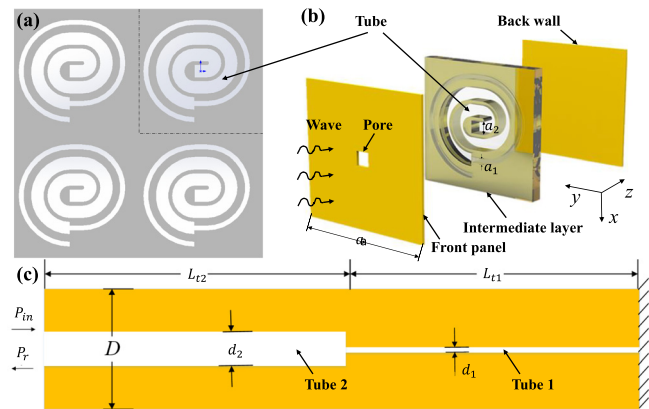


FIG. 1. (a) The sketch of the sound absorbing material with a designed unit cell; (b) the make-up of the unit cell; (c) schematic of two straight axially coupled tubes in series in analysis.

<sup>a)</sup>Email: hugeng@bit.edu.cn

between air and the solid material of the tube. The two spiral axially coupled tubes are decoupled into a straight form in the following analysis, as shown in Fig. 1(c). The diameter of the small tube (labelled as tube 1) is noted by  $d_1$ , while that of the large tube (noted as tube 2) by  $d_2$ . The lengths of the small and large tubes are  $L_{t1}$  and  $L_{t2}$ , respectively.

According to Ref. 1, the acoustic impedance at the connection with tube 2 for the small tube (tube 1) backup with a rigid wall is expressed by  $Z_1 = -jZ_1^c \cot(k_1 L_{t1})$ , where  $k_1 = \omega \sqrt{\rho_{eq1}/K_{eq1}}$  is the effective propagation constant of tube 1 and  $Z_1^c = \sqrt{\rho_{eq1} K_{eq1}}$  is its characteristic impedance.  $\rho_{eq1}$  and  $K_{eq1}$  are the effective density and the bulk modulus of air in the hollow tube derived from the visco-thermal acoustic theory<sup>29-31</sup> and given by

$$\rho_{eq1} = \rho_0 / F(\vartheta), \quad (1)$$

$$K_{eq1} = \gamma P_0 / [\gamma - (\gamma - 1)F(\vartheta'/\gamma)], \quad (2)$$

where  $\rho_0$ ,  $\gamma$ , and  $P_0$  represent the density of air, the ratio of specific heat, and the air pressure, respectively, and  $\vartheta = \mu_0 / \rho_0$ , and  $\vartheta' = \kappa_0 / (\rho_0 C_{v0})$ , with  $\mu_0$ ,  $\kappa_0$ , and  $C_{v0}$  denoting the air viscosity, thermal conductivity, and heat capacity at a constant volume, respectively. The function  $F(\eta)$  is expressed by

$$F(\eta) = 1 - 4(-j\omega/\eta)^{-1/2} G \left[ d_1 (-j\omega/\eta)^{1/2} / 2 \right] / d_1, \quad (3)$$

where the function  $G$  is defined by  $G[\xi] = J_1(\xi)/J_0(\xi)$ , with  $J_0$  and  $J_1$  being the first kind of Bessel functions of zero and first orders.

The surface impedance of tube 2 at the left entrance is expressed by

$$Z_2 = Z_1^c \frac{-jZ_{11} \cot(k_2 L_{t2}) + Z_1^c}{Z_{11} - jZ_1^c \cot(k_2 L_{t2})}, \quad (4)$$

where  $Z_{11} = Z_1/\phi_1$  and  $\phi_1 = A_1/A_2$ , with  $A_1$  and  $A_2$  being the cross-sectional areas of tube 1 and tube 2, respectively.  $k_2$  is the effective propagation constant of tube 2, evaluated using the same method as that of tube 1.

Analogously, the input impedance of sound for tube 2 can be estimated as  $Z_{in} = Z_2/\phi_2$ , with  $\phi_2$  being defined as the porosity of the unit cell. Finally, the sound absorption coefficient of the material is determined by  $\alpha = 1 - |(Z_{in} - Z_{c0})/(Z_{in} + Z_{c0})|^2$ , where  $Z_{c0}$  is the characteristic impedance of air. It is seen that full absorption requires the impedance-match condition between the material and air.<sup>26,27</sup>

The numerical simulation is also conducted using COMSOL Multiphysics<sup>TM</sup> with the Acoustic module to validate the analytical model. A plane wave with a unit amplitude impinges normally to the sample, and the sound hard boundary is imposed on the interface between air and the surface of the tube. In the computation, the cross-section of the unit cell is circular with a diameter  $D$  of 30 mm. The cross-sections of the two coupled tubes are squares with equivalent diameters of  $d_2=12$  mm and  $d_1=3$  mm, respectively, and their lengths are 860 mm and 857.5 mm, respectively, which are selected for a designed frequency of around

hundred Hz. The equivalent diameter  $d$  used in the analytical model is related to the side length of the square  $a$  used in the computation and experiment by  $a^2 = \pi d^2/4$ . A square pore in the middle of the front panel connects tube 2 in the intermediate layer [Fig. 1(b)]. In the analytical model and numerical simulation, the thickness of the front panel and the back wall is neglected. The absorption coefficient is determined by  $\alpha = 1 - |r|^2$ , with  $r$  representing the complex reflection coefficient.

Figure 2 shows the absorption coefficient of the proposed panel with two absorption peaks designed at 81 Hz and 106 Hz. The absorption coefficient of the sample is greater than 0.8 over a frequency band of 36 Hz from 76 Hz to 112 Hz. The total thickness of the system is 117.1 mm which is only 1/38.5 of the wavelength at 76 Hz. The comparison of the absorption coefficient between the analytical model and the simulation is also shown in Fig. 2, where a good agreement is observed.

The experiment is also performed to further verify the sound absorption capacity of the proposed material. A sample of circular unit cell with a diameter of 100 mm is fabricated by the 3D printing technique, and this size of the unit cell is chosen to meet the measurement condition using a B&K 4206T impedance tube.

In the experiment, the cross-sections of the tubes are of square shape for easy fabrication, as shown in the inset in Fig. 3. The geometric parameters of tube 1 and tube 2 are  $L_{t1} = 103$  mm and  $d_1 = 2.68$  mm and  $L_{t2} = 107$  mm and  $d_2 = 25.3$  mm, respectively. The thickness of the front panel and the back wall is 0.2 mm, and the total thickness of the sample is 22.7 mm. With this geometry, the two absorption peaks are designed at 734 Hz and 856 Hz, respectively. The experimental result shows that the measured acoustic absorption coefficient is greater than 0.8 over a frequency band of 182 Hz from 708 Hz to 890 Hz with the wavelength to thickness ratio of 21.3, and the sample is therefore on the subwavelength scale. The experimental result agrees with the predictions by both the analytical model and the numerical simulation. It is also noted that the frequency bandwidth of the experiment is wider than that of the prediction and the discrepancy between the measurement and the prediction is large in a high frequency range. This is probably due

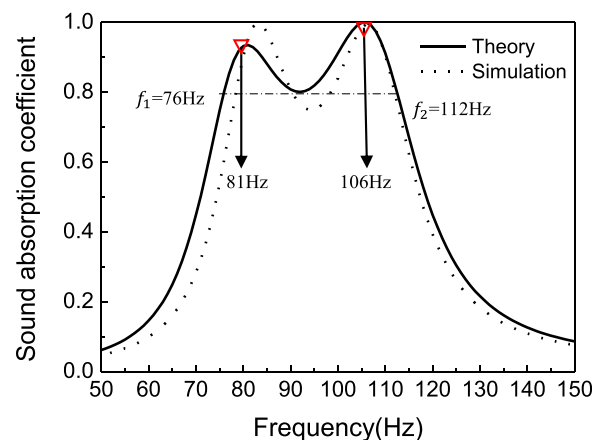


FIG. 2. Comparison between the analytical and numerical models on the absorption coefficient of the circular panel as a function of frequency with two resonant frequencies designed at 81 Hz and 106 Hz.

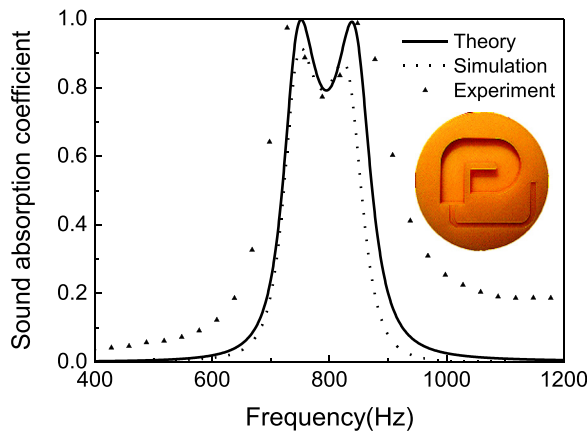


FIG. 3. Comparison between the measured and computed absorption coefficients for the proposed material with two resonant frequencies designed at 734 Hz and 856 Hz.

to additional energy consumption by the rough surface during 3D printing,<sup>32–34</sup> which is not considered in the analytical model and the numerical simulation.

It is demonstrated that by coupling two axially connected tubes, we can broaden the frequency range of high absorption induced by resonances. It is interesting to examine the geometry of the tube for achieving better sound absorption. In the following, we set the size of the unit cell, the length, and the diameter of tube 2 be fixed at  $D = 100$  mm,  $L_{r2} = 860$  mm, and  $d_2 = 32$  mm, and examine the influence of the length and the diameter of tube 1 on the sound absorption. Figure 4 shows the variation in the absorption coefficient as a function of the normalized tube length  $l_t = L_{r1}/L_{r2}$  and diameter  $d = d_1/d_2$ . It is seen that the absorption coefficient will be greater than 0.9 when the length of the small tube varies from  $0.89L_{r2}$  to  $0.99L_{r2}$  and its diameter of the cross-section varies from  $0.23d_2$  to  $0.3d_2$ . Based on the result in Fig. 4, we can find the optimized geometric parameters of the small tube when those of the large tube are fixed.

In fact, there are five geometric parameters of the two axially coupled tubes,  $D$ ,  $d_1$ ,  $d_2$ ,  $L_{r1}$ , and  $L_{r2}$ , influencing the sound absorption of the material. In the above simulation,

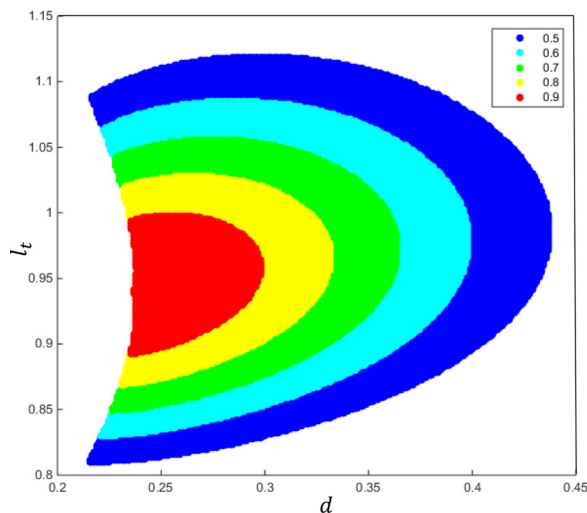


FIG. 4. Absorption coefficient as a function of the normalized length and the diameter of the small tube designed for a targeted frequency of around 100 Hz.

the size of the unit cell  $D = 100$  mm is fixed, which prevents from further thickness reduction. We will set the lengths of two tubes be fixed at  $L_{r1} = 857.5$  mm and  $L_{r2} = 860$  mm, meaning that two absorption peaks are designed at around 100 Hz, and examine the influence of the normalized unit cell size  $D' = D/L_{r2}$  and diameters of the tubes  $d'_1 = d_1/L_{r2}$  and  $d'_2 = d_2/L_{r2}$  on the wavelength to thickness ratio and frequency bandwidth for a given value of the minimum absorption coefficient (0.8) in the following computation.

Figure 5(a) shows the wavelength to thickness ratio as a function of the unit cell size and the tube diameters. Here, the wavelength to thickness ratio is defined by the wavelength of the first absorption peak to the sample thickness. As observed in Fig. 5(a), this ratio can be as high as 169.9; however, the corresponding frequency bandwidth becomes very narrow of only 5 Hz, as shown in Fig. 5(b).

Figure 5(b) shows the frequency bandwidth as a function of the normalized tube diameter and the unit cell size, while the lengths of the tubes remain the same as those in Fig. 5(a); the absorption coefficient is also set to be larger than 0.8. It is seen that the frequency bandwidth of the designed material can be as high as 36 Hz, and the corresponding wavelength to thickness ratio is about 38.5, which was examined in the above paragraph.

It is found from Figs. 5(a) and 5(b) that achieving good sound absorption with a thin thickness and a large frequency

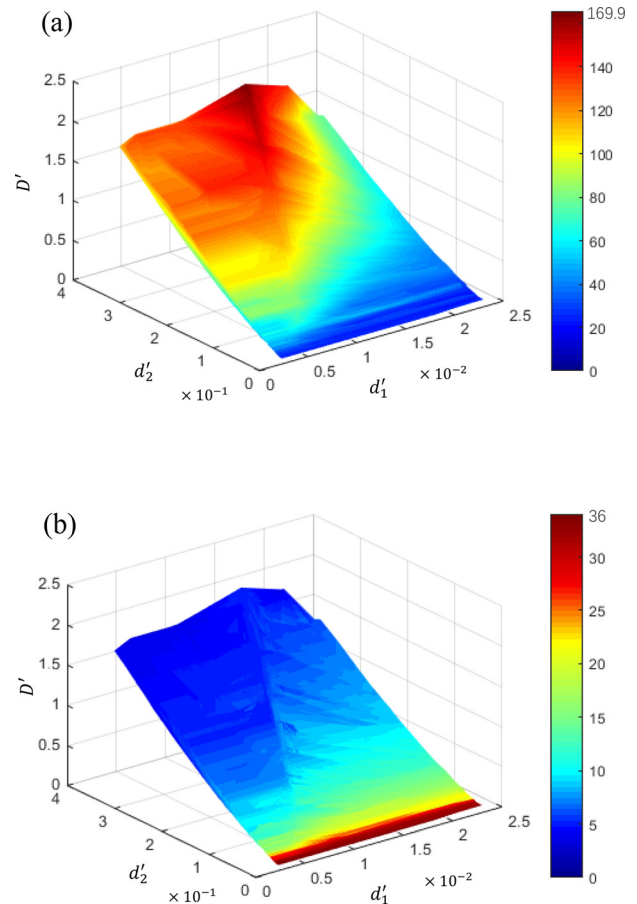


FIG. 5. Wavelength to thickness ratio (a) and frequency bandwidth of the material (b) as a function of the normalized unit cell size  $D' = D/L_{r2}$  and the diameters of tubes  $d'_1 = d_1/L_{r2}$  and  $d'_2 = d_2/L_{r2}$  designed for a targeted frequency of around 100 Hz with a minimum absorption of 0.8.

bandwidth simultaneously is difficult, which has been recently demonstrated through the casualty principle.<sup>35</sup> In fact, in order to achieve a good sound absorption performance, materials need enough cavity volume, a wider frequency bandwidth, and a larger sample thickness. We should consider the balance between the frequency bandwidth and the wavelength-to-thickness ratio of the material for a targeted application.

A sound absorbing material with a designed unit cell of two axially coupled tubes connected in series has been proposed. The axially coupled tubes are coiled in a plane to further reduce the sample thickness. This material is shown to be able to absorb low frequency sound energy with a relatively large frequency bandwidth and thin thickness. The influence of geometric parameters of the tubes on sound absorption is also analyzed. By proper design, a material with a wavelength to thickness ratio of 169.9 for sound of hundred Hz can be designed. However, it is also found that a compromise should be made among the absorption coefficient, bandwidth, and sample thickness at low frequency. The result may provide insights into a new material design for low frequency sound absorption.

We acknowledge the funding support from the Natural Science Foundation (Grant No. 11472044, 11221202, 11632003, and 11521062) and from 111 Project (B16003).

<sup>1</sup>J. Allard and N. Atalla, *Propagation of Sound in Porous Media: Modelling Sound Absorbing Materials 2e[M]* (John Wiley & Sons, 2009).  
<sup>2</sup>H. Meng, Q. B. Ao, S. W. Ren, F. X. Xin, H. P. Tang, and T. J. Lu, "Anisotropic acoustical properties of sintered fibrous metals," *Compos. Sci. Technol.* **107**, 10–17 (2015).  
<sup>3</sup>D. Lafarge, P. Lemariniere, J. F. Allard, and V. Tarnow, "Dynamic compressibility of air in porous structures at audible frequencies," *J. Acoust. Soc. Am.* **102**(4), 1995–2006 (1997).  
<sup>4</sup>M. A. Biot, "Theory of propagation of elastic waves in a fluid-saturated porous solid. I. Low-frequency range," *J. Acoust. Soc. Am.* **28**(2), 168–178 (1956).  
<sup>5</sup>P. Wei, C. Croëne, S. T. Chu, and J. Li, "Symmetrical and anti-symmetrical coherent perfect absorption for acoustic waves," *Appl. Phys. Lett.* **104**(12), 121902 (2014).  
<sup>6</sup>T. Dupont, P. Leclaire, O. Sicot, X. L. Gong, and R. Panneton, "Acoustic properties of air-saturated porous materials containing dead-end porosity," *J. Appl. Phys.* **110**(9), 094903 (2011).  
<sup>7</sup>Z. Bo and C. Tianning, "Calculation of sound absorption characteristics of porous sintered fiber metal," *Appl. Acoust.* **70**(2), 337–346 (2009).  
<sup>8</sup>S. Felix, B. Sapoval, M. Filoche, and M. Asch, "Enhanced wave absorption through irregular interfaces," *Europhys. Lett.* **85**(1), 14003 (2009).  
<sup>9</sup>C. Wang, L. Cheng, J. Pan, and G. Yu, "Sound absorption of a micro-perforated panel backed by an irregular-shaped cavity," *J. Acoust. Soc. Am.* **127**(1), 238–246 (2010).  
<sup>10</sup>W. H. Chen, F. C. Lee, and D. M. Chiang, "On the acoustic absorption of porous materials with different surface shapes and perforated plates," *J. Sound Vib.* **237**(2), 337–355 (2000).  
<sup>11</sup>A. Climente, D. Torrent, and J. Sánchez-Dehesa, "Omnidirectional broadband acoustic absorber based on metamaterials," *Appl. Phys. Lett.* **100**(14), 144103 (2012).

<sup>12</sup>S. Liu, W. Chen, and Y. Zhang, "Design optimization of porous fibrous material for maximizing absorption of sounds under set frequency bands," *Appl. Acoust.* **76**, 319–328 (2014).  
<sup>13</sup>X. Xu, P. Li, X. Zhou, and G. Hu, "Experimental study on acoustic subwavelength imaging based on zero-mass metamaterials," *Europhys. Lett.* **109**(2), 28001 (2015).  
<sup>14</sup>S. Yao, X. Zhou, and G. Hu, "Investigation of the negative-mass behaviors occurring below a cut-off frequency," *New J. Phys.* **12**(10), 103025 (2010).  
<sup>15</sup>Y. Chen, G. Huang, X. Zhou, G. Hu, and C. T. Sun, "Analytical coupled vibroacoustic modeling of membrane-type acoustic metamaterials: Membrane model," *J. Acoust. Soc. Am.* **136**(3), 969–979 (2014).  
<sup>16</sup>J. Mei, G. Ma, M. Yang, Z. Yang, W. Wen, and P. Sheng, "Dark acoustic metamaterials as super absorbers for low-frequency sound," *Nat. Commun.* **3**, 756 (2012).  
<sup>17</sup>M. Yang, C. Meng, C. Fu, Y. Li, Z. Yang, and P. Sheng, "Subwavelength total acoustic absorption with degenerate resonators," *Appl. Phys. Lett.* **107**(10), 104104 (2015).  
<sup>18</sup>S. Yao, P. Li, X. Zhou, and G. Hu, "Sound reduction by metamaterial-based acoustic enclosure," *AIP Adv.* **4**(12), 124306 (2014).  
<sup>19</sup>G. Ma, M. Yang, S. Xiao, Z. Yang, and P. Sheng, "Acoustic metasurface with hybrid resonances," *Nat. Mater.* **13**(9), 873–878 (2014).  
<sup>20</sup>Y. Duan, J. Luo, G. Wang, Z. H. Hang, B. Hou, J. Li, P. Sheng, and Y. Lai, "Theoretical requirements for broadband perfect absorption of acoustic waves by ultra-thin elastic meta-films," *Sci. Rep.* **5**, 12139 (2015).  
<sup>21</sup>Z. Liang, T. Feng, S. Lok, F. Liu, K. B. Ng, C. H. Chan, J. Wang, S. Han, S. Lee, and J. Li, "Space-coiling metamaterials with double negativity and conical dispersion," *Sci. Rep.* **3**, 1614 (2013).  
<sup>22</sup>T. Frenzel, J. D. Brehm, T. Bückmann, R. Schittny, M. Kadic, and M. Wegener, "Three-dimensional labyrinthine acoustic metamaterials," *Appl. Phys. Lett.* **103**(6), 061907 (2013).  
<sup>23</sup>Y. Li, B. Liang, X. Tao, X. F. Zhu, X. Y. Zou, and J. C. Cheng, "Acoustic focusing by coiling up space," *Appl. Phys. Lett.* **101**(23), 233508 (2012).  
<sup>24</sup>Y. Xie, B. I. Popa, L. Zigoneanu, and S. A. Cummer, "Measurement of a broadband negative index with space-coiling acoustic metamaterials," *Phys. Rev. Lett.* **110**(17), 175501 (2013).  
<sup>25</sup>Y. Xie, W. Wang, H. Chen, A. Konneker, B. I. Popa, and S. A. Cummer, "Wavefront modulation and subwavelength diffractive acoustics with an acoustic metasurface," *Nat. Commun.* **5**, 5553 (2014).  
<sup>26</sup>X. Cai, Q. Guo, G. Hu, and J. Yang, "Ultrathin low-frequency sound absorbing panels based on coplanar spiral tubes or coplanar Helmholtz resonators," *Appl. Phys. Lett.* **105**(12), 121901 (2014).  
<sup>27</sup>Y. Li and B. M. Assouar, "Acoustic metasurface-based perfect absorber with deep subwavelength thickness," *Appl. Phys. Lett.* **108**(6), 063502 (2016).  
<sup>28</sup>J. P. Groby, R. Pommier, and Y. Auréan, "Use of slow sound to design perfect and broadband passive sound absorbing materials," *J. Acoust. Soc. Am.* **139**(4), 1660–1671 (2016).  
<sup>29</sup>M. R. Stinson, "The propagation of plane sound waves in narrow and wide circular tubes, and generalization to uniform tubes of arbitrary cross-sectional shape," *J. Acoust. Soc. Am.* **89**(2), 550–558 (1991).  
<sup>30</sup>Y. Champoux and J. F. Allard, "Dynamic tortuosity and bulk modulus in air-saturated porous media," *J. Appl. Phys.* **70**(4), 1975–1979 (1991).  
<sup>31</sup>D. L. Johnson, J. Koplik, and R. Dashen, "Theory of dynamic permeability and tortuosity in fluid-saturated porous media," *J. Fluid Mech.* **176**, 379–402 (1987).  
<sup>32</sup>V. Bontozoglou and G. Papapolymerou, "Laminar film flow down a wavy incline," *Int. J. Multiphase Flow* **23**(1), 69–79 (1997).  
<sup>33</sup>S. G. Kandlikar, D. Schmitt, A. L. Carrano, and J. B. Taylor, "Characterization of surface roughness effects on pressure drop in single-phase flow in minichannels," *Phys. Fluids* **17**(10), 100606 (2005).  
<sup>34</sup>G. Gamrat, M. Favre-Marinet, S. Le Person, R. Baviere, and F. Ayela, "An experimental study and modelling of roughness effects on laminar flow in microchannels," *J. Fluid Mech.* **594**, 399–423 (2008).  
<sup>35</sup>M. Yang, S. Chen, C. Fu, and P. Sheng, "Optimal sound absorbing structures," preprint [arXiv:1609.09561](https://arxiv.org/abs/1609.09561) (2016).